

Nanoscale

Accepted Manuscript



This is an *Accepted Manuscript*, which has been through the Royal Society of Chemistry peer review process and has been accepted for publication.

Accepted Manuscripts are published online shortly after acceptance, before technical editing, formatting and proof reading. Using this free service, authors can make their results available to the community, in citable form, before we publish the edited article. We will replace this *Accepted Manuscript* with the edited and formatted *Advance Article* as soon as it is available.

You can find more information about *Accepted Manuscripts* in the [Information for Authors](#).

Please note that technical editing may introduce minor changes to the text and/or graphics, which may alter content. The journal's standard [Terms & Conditions](#) and the [Ethical guidelines](#) still apply. In no event shall the Royal Society of Chemistry be held responsible for any errors or omissions in this *Accepted Manuscript* or any consequences arising from the use of any information it contains.

ARTICLE

Contact Angles on Surfaces Using Mean Field Theory: Nanodroplet vs. Nanoroughness

Cite this: DOI: 10.1039/x0xx00000x

A. P. Malanoski,^a B. J. Johnson^a and J.S. Erickson^a,

Received 00th January 2012,
Accepted 00th January 2012

DOI: 10.1039/x0xx00000x

www.rsc.org/

With emerging systems and applications accessing features within the nano regime, whether due to droplet size or feature size, understanding the wetting behaviours for these materials is an area of ongoing interest. Theoretical studies, providing a fundamental understanding of how contact angle behaviour changes at these length scales, are important to further such work. This study provides a comprehensive examination of the application of lattice density functional theory (LDFT) to a pillared surface to confirm the suitability of LDFT for studying more complex surfaces. Incorporation of the correct level of detail for the fluid-wall interaction was found to produce all of the qualitative changes that have been observed in off-lattice theories. Though previous reports have provided apparently conflicting results, the more comprehensive examination of feature sizes provided here demonstrates that those behaviours are consistent with one another. The well-studied failure of macroscopic models that results from non-negligible line tension contributions and small droplet to feature size ratios was demonstrated with LDFT. Furthermore, the failure of macroscopic models resulting upon reduction in feature size, which has been considered less often, is clearly demonstrated. A key assumption of the macroscopic models is the consistent interaction between surface and fluid regardless of the flatness or roughness of the surface. The density functional results presented here show that, for the smallest features, this is not the case and demonstrate that macroscopic models do not predict the correct contact angle for droplets of any size on nano rough surfaces.

Introduction

The application of microscopic approaches using density functional formalisms for evaluation of nanodrops on surfaces has been the topic of several papers. Young's classic description of wetting angles was developed over 200 years ago. The equation relates the contact angle (θ) to the solid-vapour (γ_{vw}), solid-liquid (γ_{wl}), and liquid-vapour (γ_{vl}) free energies while neglecting contributions from the intersection of the three phases.¹

$$\cos \theta = \frac{\gamma_{vw} - \gamma_{wl}}{\gamma_{vl}} \quad (1)$$

This classic result is reasonably accurate and routinely used for macroscale droplets on flat, homogenous surfaces that have negligible contributions from the intersection of the phases. Several studies have produced modifications to equation (1) to quantitatively account for the contribution of the phase intersections.²⁻⁶ It was found that, as droplet size decreases into the micro scale range, equation (1) holds, while for cases focused on droplets approaching the nanoscale, inclusion of contributions from the intersection of the

phases becomes important. Extensions to this simple model were also developed to address chemical and physical heterogeneity (Cassie-Baxter and Wenzel models, respectively). These models are focused on behaviour of large droplets and ignore line tension contributions.⁷⁻⁹ The Cassie-Baxter form initially developed for chemical heterogeneity on flat surfaces has been further extended for application to systems with physical heterogeneity by assuming that one surface within the system (representing air) has a 180° contact angle. These two models predict two very different types of droplets on rough surfaces. In the Cassie-Baxter model, the droplet sits on top of the structure with a vapour phase surrounding the features. In the Wenzel model, the droplet is in intimate contact with the entire surface. Several excellent reviews cover work on a range of issues that relate to droplets considered using these models.¹⁰⁻¹²

Some effort has been made to more rigorously define the relationship between contact angle and free energies, but these definitions are rarely applied to physical studies. The Wenzel and Cassie models have been shown to be special cases of these more rigorous and general relationships.^{13, 14} Depending on real system

conditions, a Wenzel-type drop or a Cassie-type drop will be more energetically favourable. Conditions under which the application of these models may fail have also been actively discussed in the literature.¹⁴⁻¹⁷ These failures are most often related to systems for which the critical assumptions of the models fail to hold. A critical assumption, for example, is that the droplet is much larger than the size of surface variations, whether physical or chemical. There are other assumptions for these models that, to date, have not been encountered in experimental systems. As capabilities and systems continue to evolve, assumptions regarding the composition of the surface and the accuracy of representing surface interactions based on the flat surface assumption may become problematic.

Although the effects of metastability and hysteresis often prevent the observation of the lowest energy configuration for real droplets, thermodynamic considerations are still important to understanding the behaviours observed for droplets on surfaces. Density functional formalisms allow a detailed examination of a range of small drop sizes, incorporate molecular interactions, allow study of metastable as well as stable states, and provide a point of comparison for other theories. While small droplet behaviour will deviate from that predicted by the macroscopic models, density functional formalisms with the proper level of detail can capture those deviations. Formalisms capturing varying levels of detail have led to the generation of several different models.¹⁸⁻²¹ A lattice density functional study found that trends in overall behaviour for nanodroplets could be qualitatively predicted by simple theories while the physically observed contact angles were shifted to smaller than predicted values.²¹ A more detailed off lattice 2D density functional study found similar behaviour for some wall-fluid interaction strengths.^{18, 19} This study also identified a behaviour that was the opposite of that described by the simple theories for some of the cases considered. This model considered conditions (wall-fluid interaction strengths, height, shape, width, and spacing of features) that were highly different from the other study in addition to the inherent differences in spatial detail. It is important, when making these comparisons, to understand whether differences in predictions are due to changes in variables describing the system or due to the difference in lattice versus off lattice approach. Lattice simulations are significantly faster than off lattice, but, if details critical to modelling real systems are not present, the benefit of faster solutions is not relevant.

The effort described here applies a lattice density functional formalism to a broader study of variations in surface configuration and droplet size. We sought to access a range over which the contact angle of a droplet is not predicted by the Cassie-Baxter or Wenzel equations. A broader study of the variations in surface configuration also provides better context for previous theoretical work and accounts for the apparent disagreement in observed trends with previous off lattice studies. A unique advantage of lattice density functional formalisms is the ability to explore model systems that, while less realistic, offer a clearer understanding of the influence of different levels of detail. It is also possible to calculate contact angles by several different methods allowing for direct comparison to other studies. Here, the use of a lattice density functional model allows exploration of a large number of physical features and interaction conditions in order to provide an overview of important effects as droplet and/or physical feature size enter the nano regime.

Methods

Lattice model

A 3D single occupancy lattice density functional model developed previously was used to study the wetting behaviour on various

surface structures.²² The model allows for a mean field square-well-type attraction for nearest neighbour sites on a lattice. For this study, a simple cubic lattice was used. The grand potential function, $\beta\Omega[\rho]$, of M lattice sites and l_{spe} species, which is 1 (one) for this study, is represented by the following expression:

$$\beta\Omega[\rho] = \sum_i^M \left[\left(1 - \sum_k^{l_{spe}} \rho_i^k\right) \ln\left(1 - \sum_k^{l_{spe}} \rho_i^k\right) + \sum_k^{l_{spe}} \left(\rho_i^k \ln \rho_i^k + \rho_i^k \beta V_i^k - \rho_i^k \beta \mu_i^k + \frac{\beta}{2} \sum_m^{N_e} \sum_n^{l_{spe}} \epsilon_{d(i,m)}^{kn} \rho_i^k \rho_{I(i,m)}^n \right) \right] \quad (2)$$

where ρ_i^k is the density of species k at lattice site i , β is $1/kT$ where T is the temperature and k is Boltzmann's constant, V_i^k is the external potential acting on species k at lattice site i , μ_i^k is the chemical potential of species k at lattice site i , N_e is the number of interacting neighbours for the chosen lattice (which in the case of a simple cubic lattice is 6), and $d(i,m)$ and (i,m) are lattice dependent functions to obtain neighbor positions. The critical temperature for this model is $kT_c = -\rho_c N \epsilon_1^{ff}/2$ where the critical density is $\rho_c = 0.5$ and $\epsilon_1^{ff} = -1.0$ is the mean field fluid interaction which results in $kT_c = 1.5$. The model was studied at a single temperature, $T/T_c = 0.234$. The wall sites were not considered to be a species for modelling purposes. It was determined to be more efficient to compute the contribution from wall sites for each individual species at each lattice site. These values were added to the βV_i^k value for that lattice site. This means that the wall-fluid interactions only needed to be calculated once for a given solution. The potentials used are described below.

A single temperature was selected for evaluation at $T/T_c = 0.234$ to facilitate comparison to other studies while limiting the number of cases to be evaluated under this effort. The range of possible temperatures for the model is limited by the critical temperature of the system. It should be noted that the form of the data utilized (presented as the interaction energy required to obtain a given contact angle on a flat surface) allows for generalization of the results to other temperatures.

The partial derivatives with respect to the species density at each site can be determined from the grand potential functional:

$$\frac{\partial(\beta\Omega[\rho])}{\partial \rho_i^k} = \ln \rho_i^k - \ln\left(1 - \sum_k^{l_{spe}} \rho_i^k\right) + \beta V_i^k - \beta \mu_i^k + \frac{\beta}{2} \sum_m^{N_e} \sum_n^{l_{spe}} \epsilon_{d(i,m)}^{kn} \rho_{I(i,m)}^n \quad (3)$$

At equilibrium, all these partial derivatives equal zero, and Eq. 2 is at its global minimum. In practice it is possible to solve for a local minimum rather than the global minimum depending on the initial density values assigned to all lattice sites. We interpret the local minima as metastable equilibrium points. Physical droplet DFT solutions are solved in the NVT ensemble where the Helmholtz free energy describes the system. This ensemble has additional constraints that the total N of each species is constant. Using undetermined Lagrangian multipliers these constraints can be incorporated and the partial derivatives can be expressed as:

$$\frac{\partial(\beta F[\rho])}{\partial \rho_i^k} = \ln \rho_i^k - \ln\left(1 - \sum_k^{l_{spe}} \rho_i^k\right) + \beta V_i^k + \alpha^k + \frac{\beta}{2} \sum_m^{N_e} \sum_n^{l_{spe}} \epsilon_{d(i,m)}^{kn} \rho_{I(i,m)}^n \quad (4)$$

where

$$\alpha^k = \frac{-1}{M} \sum_i^M \left[\ln \rho_i^k - \ln \left(1 - \sum_k^{lspe} \rho_i^k \right) + \beta V_i^k + \frac{\beta}{2} \sum_m^{Ne} \sum_n^{lspe} \epsilon_{d(i,m)}^{kn} \rho_{l(i,m)}^n \right] \quad (5)$$

A Picard iteration scheme was used to solve for the site densities at the specified chemical potential using the set of partial derivatives in Eq. 3 or for given fixed amounts of species using Eq. 4 and 5. Density functional theory is advantageous in this regard because the appropriate free energy is easily computed, and a global minimum can be selected from any local minima generated using different initial conditions.

The wall-fluid interaction was modelled in one of two ways to study the effect of including different levels of detail. A square well potential interaction between nearest-neighbour fluid sites to all wall sites (SW potential) was used as a less accurate model and a potential adopted from a previous study was used to better represent the solid-fluid interaction.²¹ This potential consists of a Lennard-Jones 12-6 potential for sites in pillar structures on top of a surface represented by an integrated wall potential (LJ potential). The 12-6 potential was cut off at 8σ where σ is the distance of the lattice site separation and also the effective diameter of fluid molecules. For most of the studies a simple square well nearest neighbour model was used for the fluid-fluid interaction. This model is sufficient to provide the necessary vapour-liquid phase interaction. A simple stepped interaction considering the closest three lattice sites was also evaluated. This model did not result in significant perturbation to the observed qualitative behaviours. While the exclusion of mid- and long-range fluid-fluid interactions could result in oversimplification, more complicated potentials would diminish the benefit of using the lattice rather than off lattice formalisms. Comparison to established models of behaviour on flat surfaces was used for validation of this approach (see Results).

Several types of DFT solutions were performed for this work. The x -dimension shall always refer to the position perpendicular to the wall while y - and z -dimensions are parallel to the surface. When a DFT model box has y and z different lengths, the z -dimension is assigned to the shorter box length. NVT ensemble DFT solutions are used to determine a stable or metastable configuration of a droplet, that is either fully 3-dimensional (box size: $150\sigma \times 200\sigma \times 200\sigma$) or pseudo 2-dimensional (p2D; box sizes ranged from: $150\text{--}500\sigma \times 200\text{--}880\sigma \times$ length of one to four unit cells). For these cases, initial starting configurations used a hemispherical cap region placed at the top or base of the features.

An alternate method for obtaining contact angles is to use the DFT model to obtain values for γ_{vw} , γ_{lw} , and γ_{vl} on a given heterogeneous surface and use them in Young's equation to produce a contact angle prediction. Young's equation is normally considered to apply to a flat surface where estimations of the various free energies are possible, but it can be used for any surface if a method is available to determine the free energy values. The contact angle calculated represents the large droplet size limit since line tension contributions are ignored. For this method, the DFT model was solved in the grand ensemble (box size: $15\text{--}20\sigma$ + height of feature x , one or two unit cells of pattern). Three different solution conditions were used: (1) a bulk fluid with a vapour-liquid interface present, (2) a liquid above a surface, and (3) a vapour above a surface. These cases provide the liquid-vapour, liquid-wall, and vapour-wall free energies. Young's equation is then used to calculate a contact angle. The bulk fluid solution is required only once for a given temperature condition. Initial configurations for each wall interaction case consist of a thin layer of liquid near wall for vapour, a thick layer of vapour near wall, and the density profile that was the solution of the previous run. Unless reported otherwise, the features used in the DFT model

are square pillars described by s for the side length, d for the separation between pillars, and h for the height.

Results

Flat surfaces: methods for calculating contact angles

In order to test the methods used here, we will first consider predictions from the models for flat surfaces. There are several approaches to solving for contact angles. Fundamentally, determinations involve either application of Young's equation (for systems where free energies are calculated) or construction of a droplet configuration from which the contact angle can be measured. Variations on the latter approach are possible due to the differences in methods used for generation of droplet constructs. The configuration of fully 3-dimensional (3D), pseudo 2-dimensional (p2D), or 2-dimensional (2D) droplets can be solved using lattice density functional theory. A p2D droplet results from a 3D droplet in which one of the solution box lengths is much shorter than the others and the initial configuration forms a periodic infinite cylinder in that direction. Though these systems do not reflect physically reproducible conditions, the use of a 2D or p2D rather than the full 3D droplet is attractive because the solutions require less computation time and allow larger droplet diameters to be studied. Faster solution times also allow for more complete exploration of the metastable droplet states possible in lattice density functional models. The p2D DFT solution is typically more useful than a 2D DFT solution because identical surface structures can be evaluated under the 3D configuration. This is not necessarily the case for strictly 2D DFT solutions. Unlike droplet constructs, contact angles calculated using Young's equation with DFT free energies neglect line tension contributions (but not other potential contributions) and represent the contact angle for larger droplets on the nano rough surfaces studied. The DFT solution box for this technique can be significantly smaller and may be solved in the grand ensemble providing a great reduction in computation time. Using this approach, contact angles can be calculated for a range of wall-fluid interaction strengths (for example, from wetting to non-wetting) in the time needed to solve a single p2D droplet case at one wall-fluid interaction strength.

Figure 1 presents results for 3D and p2D droplets on a flat surface. These results are compared to those from application of Young's equation, which has no dependence on droplet size, with DFT free energies for two types of wall-surface interaction, the LJ and SW potentials described above. The value of the wall-fluid interaction for the individual cases was selected so that application of Young's Equation with DFT free energies would produce a similar contact angle $\sim 101.8^\circ$ (Supplemental Figure S1 has results for the LJ potential with a more wetting surface showing similar trends). The radius reported is for the area of the fluid ($\rho > 0.5$) in contact with the surface. As the radius is increased, 3D and p2D DFT solutions approach the same limiting contact angle. The contact angle deviates from the limiting value at the smallest droplet sizes, in agreement with previous findings. The contact angles and radius from the DFT solutions can be used with a simple model that accounts for the contribution from line tension:⁴

$$\cos \theta_i = \frac{\gamma_{vw} - \gamma_{lw}}{\gamma_{vl}} - \frac{\tau}{\sigma R} \quad (6)$$

This is the simplest expression used; it does not explicitly describe the influence of surface shape, droplet shape, or local contact angle. Nevertheless, in all cases, the deviations from the limiting contact angle value as droplet size decreases are well described by the general form (Table 1). The different potentials (LJ and SW) have similar but not identical values. The change in droplet shape due to application of 3D versus p2D or use of a different surface potential strength alters the calculated line tension in agreement with predicted behaviour from earlier models.⁴⁻⁶

Using Young's equation with DFT free energies gives a contact angle value 101.7° for the LJ potential and 101.9° for the SW potential. This should be the contact angle of physically simulated droplets as the droplet size becomes very large; however, simulated droplets may report a slightly different angle due to approximations used in computing contact angles. The method used to calculate the contact angle from a DFT solution of a physical droplet was initially adopted from an earlier study.²¹ The approach involves estimating the tangent line to the curvature of the droplet near the surface. The contact angle is then the angle between this line and the surface. The tangent line is determined by linear regression of the radii of the droplet in four successive parallel planes two lattice sites above the tallest feature on the surface ($x = 2$).

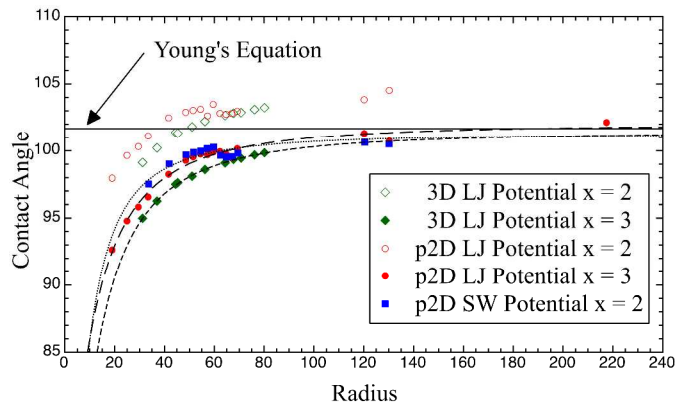


Figure 1. Contact angle versus the droplet radius from 3D simulations on a flat surface (diamonds), pseudo 2D droplet simulations using the LJ potential (circles), pseudo 2D droplet simulations using the SW potential (squares), and simulation free energies with Young's equation (solid line). The filled symbols for the integrated potential use the alternative method of calculating droplet contact angle.

Table 1. Line tension parameters from equation 6.

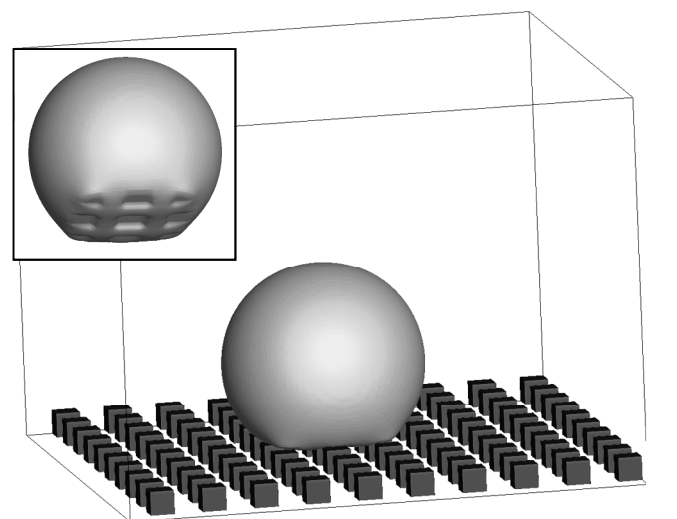
Droplet Type	Potential		Line Tension Parameter
	Type	Strength	
p2D	LJ	-0.1	-2.35
p2D	SW	-0.4561	-2.36
3D	LJ	-0.1	-3.38
p2D	LJ	-0.12	-1.74

The DFT solutions using the SW potential have droplet contact angles that are in good agreement with Young's equation using the chosen method, but the LJ potential does not. Figure 1 also presents results for the LJ potential if the four planes examined start 3 lattice sites above the tallest feature on the surface ($x=3$). The contact angles for the droplets under this analysis are reduced by roughly 2°

and are in better agreement with the contact angle determined from Young's equation with DFT free energies. General trends in behaviour remain the same regardless of the absolute contact angle measurement method applied. The caveat here applies to large size limits such as comparing DFT results to predictions from macroscopic models. When selecting the method used for estimation of contact angles in those cases, it will depend on the potential used. For the remainder of this report, contact angles for the SW potential are computed using planes starting two lattice sites above surface features. Droplet contact angles from the LJ potential surfaces are computed starting three lattice sites above the surface features with results obtained using the earlier method in parenthesis.²¹

Nanodroplet contact angles: average vs. local

While 2D and p2D DFT models are attractive due to faster solution times, a complication is introduced: different approaches (2D, p2D, and 3D) provide differing paths of contact that should be taken into account when results are compared. 2D and p2D nanodrop DFT solutions trace only sections of the entire contact line path captured by a fully 3D droplet. Figure 2 provides two views of an isodensity curve for a Cassie-like droplet on pillars based on a LJ potential ($s = d = 10\sigma$ and $h = 10\sigma$; additional curves presented in the Supplemental Information, Figure S2). The bottom of the droplet takes on a complex shape. It is possible to orient a p2D DFT solution box in a number of different ways relative to a cubically arranged pillar pattern. These orientations are equivalent with regard to surface roughness overall but represent different contact line paths for the periodic infinite cylinder that is present in a p2D solution. Two configurations are shown in Figure 3A (Case A) and 3B (Case B) representing the shortest and longest distance possible between pillars for contact line paths. Case B represents an approximate 45° rotation of Case A. The area of a pillar top is 0.25 for Case A and 0.2551 for Case B which, according to the Cassie-Baxter equation, would produce a slightly smaller contact angle in Case B. The contact angles resulting for the two cases differ significantly with Case A at 131.9° (134.9°) and Case B at 135.1° (139.4°) ($s = d = 5\sigma$ and $h = 5\sigma$). For comparison, the average contact angle for a full 3D droplet DFT solution results from a contact line that passes over geometries including the range from Case A to Case B. The contact angle, $\approx 133.0^\circ$, is similar to the average of the two p2D cases presented, $\approx 133.5^\circ$. Cases A and B were solved for several different values of s , d , and h . The local contact angle for each case varies depending on the path traced, size, and spacing of the pillars (See Supplemental Figures S3 and S4). The contact angle of Case B is always larger than that of Case A for a given surface configuration (Table 2).



potential on a surface with $s = d = h = 10\sigma$. Two views are shown, with and without the pillars rendered. Additional images provided in the Supplemental Information (Figure S2).

Nanodroplet contact angles: variation in physical heterogeneity

For flat surfaces, the type of wall-fluid potential employed has a small impact on the observed contact angles. Heterogeneous surfaces, however, display different behaviour. The use of the LJ potential for pillar sites results in smooth variations in the field experienced by fluid across the surface while the SW potential better reflects the step changes in fluid interaction that are an underlying assumption in the Cassie-Baxter model. Table 2 presents results for infinite cylinders forming a Cassie-like droplet. The contact angle changes by a large amount from one potential to another over a range of pillar sizes and heights while the fractional surface coverage by the pillars remains constant. The contact angles were computed by averaging contact angles for a selection of droplet DFT solutions where the diameter of the droplet at the surface was similar to the sizes used in an earlier study.²¹ The LJ and SW potentials also differed with regard to the conditions required to easily form a Cassie-like droplet solution. For $s = d < 10\sigma$, a Cassie-like droplet could be generated as a metastable case for $h = 5\sigma$ using the LJ potential while $h = 10\sigma$ was the minimum required for the SW potential. As $s = d$ becomes larger (10σ and 20σ) a greater pillar height was required to obtain a stable Cassie-like droplet solution. Though the interaction strengths for the two potentials were selected to produce the same flat surface contact angle, the cases presented do not produce the same trends for variations in physical heterogeneity. 3D droplets for various pillar sizes were also simulated and produced values that agreed with the corresponding cases in p2D. The contact angles determined were between the contact angles observed for the two orientations of the periodic infinite cylinder (results not shown).

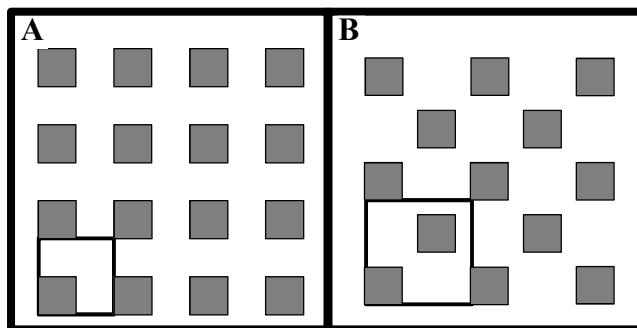


Figure 3. Pillar patterns used for simulations. Panel A has a unit cell of $2s$ where the spacing, d , between the square pillars equals the side length, s (surface fraction = 0.25), Panel B has a unit cell of $2*(1+\sqrt{2})s$ containing two square pillars with the second pillar shifted in the unit cell by $\sqrt{2}s$ in both y and z directions.

The results shown in Table 2 deviated from predictions made using the Cassie-Baxter model. This was expected due to the fact that droplet sizes considered to this point were in a size range where both line tension considerations and the ratio of droplet size to feature size may impact the contact angle. In order to explore the trends as these contributions become less significant and to determine if the Cassie-Baxter model result is approached, larger droplet sizes were studied for one surface feature size. Figure 4 presents results for a pillared surface ($s = d = 5\sigma$ and $h = 10\sigma$) using both the LJ and SW potentials. Flat surface results under the LJ potential are provided for reference. For this larger range of droplet sizes, the specific location of the droplet on the surface has an impact. The result is a varying approach to the limiting contact angle, rather than the typical smooth, monotonic approach observed for flat surfaces. This is a direct result of the changing ratio of droplet to surface feature size. It does appear that the droplets residing on the tops of the pillars are trending towards a limiting value, but the approach is slower than that observed for the flat surface. It is clear that, for the SW potential, as droplet size increases the contact angle is approaching a value in the range of 120° to 125° . It is expected even with this approximate potential that the Cassie-Baxter prediction of 143° would be the limiting value. In the case of the LJ potential, it is possible that the contact angle is approaching the Cassie-Baxter prediction, but, because of the variability in the contact angles, it is difficult to draw a definitive conclusion.

Table 2. Periodic infinite cylinder Cassie-like DFT droplet contact angles (in degrees)

Size	Height	Pattern*	Interaction Strength	Contact angle Potential LJ	Contact angle Potential SW	St. Dev.
0	0			99.6 (103.0)	99.6 (103.0)	0.23
1	10	A	LJ=-0.1 SW=-.4561	146.3 (152.5)	103.2	0.50
2	10	A	LJ=-0.1 SW=-.4561	139.5 (144.6)	110.8	0.49
3	10	A	LJ=-0.1 SW=-.4561	137.2 (141.7)	113.8	1.04
4	10	A	LJ=-0.1 SW=-.4561	136.2 (140.3)	114.5	1.11
5	5	A	LJ=-0.08	144.9 (149.4)		0.98
5	5	A	LJ=-0.1	131.1 (134.9)		1.28

5	5	B	LJ=-0.1	135.1 (139.4)		1.30
5	10	A	LJ=-0.1 SW=-.4561	133.2 (137.2)	116.5	1.25
5	10	B	LJ=-0.1 SW=-.4561	136.6 (141.0)	123.1	0.68
5	20	A	LJ=-0.1 SW=-.4561	134.0 (137.8)	116.9	1.29
5	20	B	LJ=-0.1	137.1 (141.5)		0.78
10	8	A	LJ=-0.1	130.8 (135.0)		2.39
10	8	B	LJ=-0.1	136.6 (141.6)		1.24
10	10	A	LJ=-0.1 SW=-.4561	130.8 (135.0)	120.9	2.39
10	10	B	LJ=-0.1	136.7 (141.6)		1.23
10	20	A	LJ=-0.1	131.6 (135.8)	120.5	2.45
10	20	B	LJ=-0.1	136.5 (141.6)		0.82
20	22	A	LJ=-0.1 SW=-.4561	133.2 (137.8)	119.7	3.41
20	22	B	LJ=-0.1	137.9 (143.3)		0.80
20	40	A	LJ=-0.1	132.7 (137.0)	121.1	3.32

* Patterns from Figure 3.

Droplet contact angles: droplet size independent predictions

Though the ratio of droplet size to feature size may account for effects seen with the larger drops simulated, the contact angles generated for the SW potential appear to be approaching a limit well below the Cassie-Baxter predicted value for some surface configurations. Unfortunately, it is difficult to increase the droplet or feature size further in the DFT physical droplet solutions implemented in this study. Combining DFT solution free energies with Young's equation provides a method to calculate contact angles that correspond to the limit of very large droplet to surface feature size ratios. It is expected that a transition from obeying Wenzel to Cassie-Baxter equations as the surface roughness is changed would accurately predict the DFT contact angles for droplets unless another assumption of the theories is invalid.

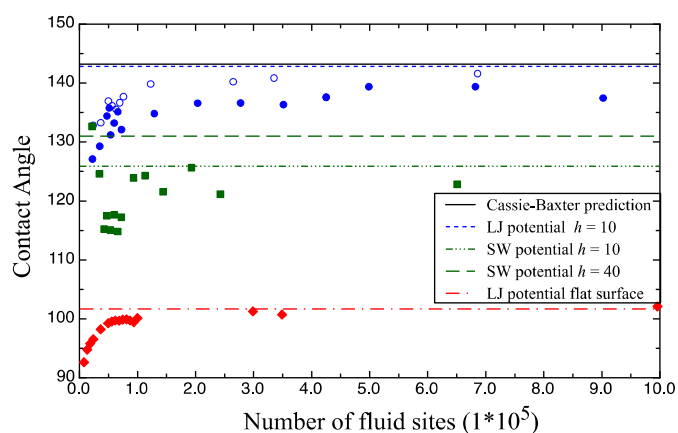


Figure 4. Contact angle versus the number of simulation sites contained within the droplet with a density greater than 0.5 from p2D simulations on a surface with $s = d = 5\sigma$ and $h = 10\sigma$. Blue circles use the LJ potential on the surface in Figure 3A (solid) and on the surface in Figure 3B (open). Green squares use the SW potential on the surface in Figure 3A. The solid line is the prediction from

Cassie-Baxter model using the contact angle on the flat surface. Simulation free energies with Young's equation were used to solve for the contact angle for the LJ potential and SW potential for the same surface structure (see legend). Also shown is the contact angle from simulation free energies with Young's equation using the SW potential when $h = 40\sigma$ and the limiting value has been reached (see legend). For reference, the red diamonds show the droplet results on the flat surface.

Under a potential that generates a low wetting flat surface contact angle ($> 90^\circ$), the angle predicted based on the DFT solutions diverges from that predicted by the Cassie-Baxter equation based on the flat surface contact angle for smaller values of s . Figure 5 demonstrates that for a given value of $s = d$, the contact angle initially increases in size then approaches a limiting value, θ_{hl} , as h increases; this last result approximates the predicted Cassie-Baxter value. The observed increase in contact angle with increasing height below hl (increasing roughness) and dependence of hl on surface roughness (changes in s and/or d) qualitatively match the behaviour predicted by the Wenzel model. The value of θ_{hl} for a given value of s , d , and h is different for the two potentials, matching the results from physical droplet simulations. The SW potential provides better agreement with the Wenzel model predictions than the LJ potential under all conditions. Contact angles for small s under the SW potential have a greater difference from the Wenzel predictions, but, as the size of s increases, the DFT solution contact angle gets closer to the Wenzel model prediction, specifically, as the region of transition to Cassie-Baxter behaviour is approached. Results for other conditions utilizing the LJ and SW potentials are provided in the Supplemental Tables S1 through S4. Often, a single thermodynamically stable contact angle is determined from the different initial configurations used. In some cases a metastable solution also appears from one of the initial configurations which corresponds to θ_{hl} for the given s and d (noted in the tables).

When θ_{hl} is plotted versus s for the LJ and SW potentials, the observed behaviours are very different (Supplemental Figure S5A and S5B). The interaction strengths used in the presented cases give a flat surface contact angle of 101.9° for the SW potential and 101.7° for the LJ potential. For the LJ potential, θ_{hl} is at a minimum value when $s = 4\sigma$ or 5σ , becomes very large for smaller values of s , and seems to be approaching some limiting value for larger values of s . For the SW potential, θ_{hl} is monotonically increasing as s increases and appears to approach some large s value limit. It is possible to plot θ_{hl} of the three largest s values versus $1/s$ and make a prediction for θ_{hl} as $s = d$ becomes very large (Supplemental Figure S5B). For the SW potential, the θ_{hl} prediction is 143.0° . In the case of the LJ potential, θ_{hl} is 145.8° . The predicted contact angle for both cases using the Cassie-Baxter equation is 143.2° .

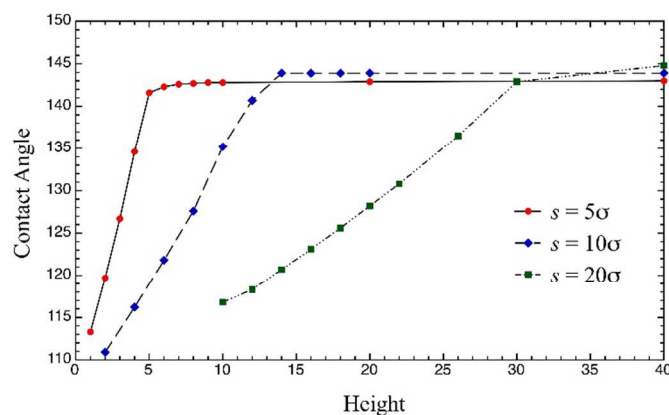


Figure 5. Contact angles from simulation free energies with Young's equation using the LJ potential with a low wetting interaction strength versus pillar height for three pillar sizes.

Returning to consideration of the droplet simulations, contact angles for 3D and p2D droplets under the SW potential (Figure 4) approach a limit in the range of 120° to 125° . This result is consistent with the contact angle, 125.9° , predicted using Young's equation with DFT free energies for the same pillar height and size. In contrast, the limiting value, θ_{hl} , from Young's prediction with DFT free energies is 131° , and the Cassie-Baxter prediction is 143° . For the LJ potential (Figure 4) under these conditions, the DFT solutions with Young's equation and Cassie-Baxter predictions are very similar, and determining which of the predictions is the limiting value is impossible.

For surface potentials that correspond to low wetting flat surfaces, the behaviour of the two potentials (LJ and SW) is qualitatively the same for increases in height with a Wenzel droplet regime that transitions to a Cassie-Baxter droplet regime. For a high wetting flat surface (contact angle $< 90^\circ$), however, the behaviour for the two potentials differs. For a surface of this type (contact angle 78°), Wenzel surface behaviour is expected. That is, the contact angle should decrease as the surface roughness increases for up to a transition point. After the transition, the behaviour should follow that of a Cassie droplet that has liquid-fluid rather than vapour-fluid between the pillars (contact angle of 0° rather than 180°). The surfaces tested with the SW potential do exhibit a decreasing contact angle with increasing values of h (i.e. increasing roughness), but, for smaller values of s , the rate of change in the contact angle is smaller than what is predicted by the Wenzel model. The LJ potential for s less than 20σ does not obey this behaviour. Instead, behaviour similar to that of the low wetting surface is observed with the contact angle increasing as height increases (Figure 6). The discrepancy between the Cassie-Baxter prediction and Young's equation with DFT free energies on tall pillars is larger than that for the low wetting case. For $s = 40\sigma$, the contact angle initially increases for the lowest values of h , then decreases with increasing h . At $s = 20\sigma$, the behaviour is difficult to determine. For a more wetting surface (flat surface contact angle of 65.5°), the behaviour previously observed for $s = 20\sigma$ is observed at $s = 5\sigma$. At $s = 20\sigma$ for the heights tested, the LJ potential has the expected behaviour - decreasing contact angle as roughness increases up to a transition to the Cassie droplet on a wet pillared surface. As the value of s increases at a fixed value of roughness, contact angles for the two potentials decrease. In the case of the SW potential, the value of s approaches the value predicted using the flat surface contact angle in Wenzel's model (Supplemental Figure S6). As the differences between the Wenzel prediction and contact angles for the LJ potential are larger, it is not clear whether the Wenzel value will be approached as s increases.

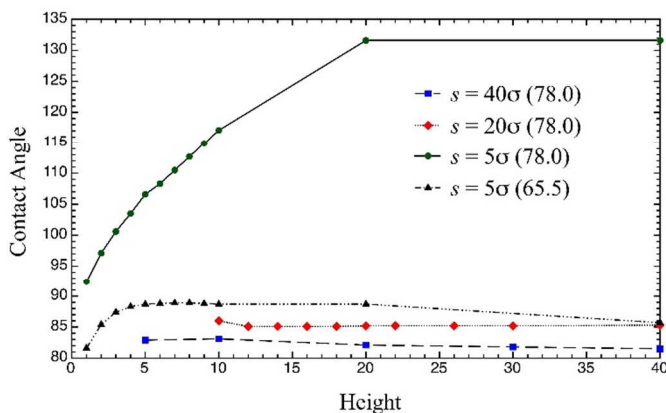


Figure 6. Contact angle versus pillar height using three pillar sizes. Contact angles were calculated from simulation free energies with Young's equation using the LJ potential with high wetting flat surface interaction strengths (< 90 degrees). The contact angle that the interaction strength would produce on a flat surface is provided in parenthesis.

Droplet contact angles: alternate implementation of Cassie's model

The results seen for Young's equation with DFT free energies suggest strongly that, when the surface features become sufficiently small, a departure from the macroscopic models, independent of droplet size, occurs. An underlying assumption of the macroscopic model is that the fluid contact surface corresponds either to flat surface or air. For real surfaces, there is a third region representing the transition between these two surfaces. When the pattern of surface features is large, the transition region represents only a small fraction of the surface and can be ignored as line tension contributions are ignored for large droplets. In the case of the pillar geometry, the transition region becomes significant as the value of s decreases.

For the SW potential, the interaction distance is limited to neighbouring sites. The transition region can be approximated to be the sites immediately surrounding a pillar and directly affected by the wall potential. This allows us to estimate a fraction of sites, $1/s$, subject to an interaction potential ranging between that of the flat surface and air. Treating this region as a third surface region and applying the Cassie-Baxter equation will produce contact angles that depend on the size of the pillar. If it is assumed that this third region interacts with the same strength as the tops of pillars, the behaviour predicted from this equation (based on the flat surface energy) qualitatively (but not quantitatively) matches the contact angles from the DFT solutions (Figure 7). If this third type of interaction strength is fitted to a few of the DFT solution values for θ_{hl} at different pillar sizes, a reasonably good fit of θ_{hl} at all pillar sizes is generated (see Figure 7). From this fit, it is clear that the contribution of this third region only becomes significant when the pillar side length is less than 100σ . Above that, the variance from the previously predicted limiting value is less than one degree.

The behaviour as pillar size changes for the LJ potential does not match that seen for a three surface Cassie model of the SW potential. This result is not unexpected as the longer range van der Waals interactions of the LJ potential provide more complicated behaviour when the size of the pillar decreases. This complication would also be expected in real systems. Because a solid site contributes to fluid interactions over greater distances, the size of the transition region is larger and extends into and away from the pillar edge in a more complex manner.

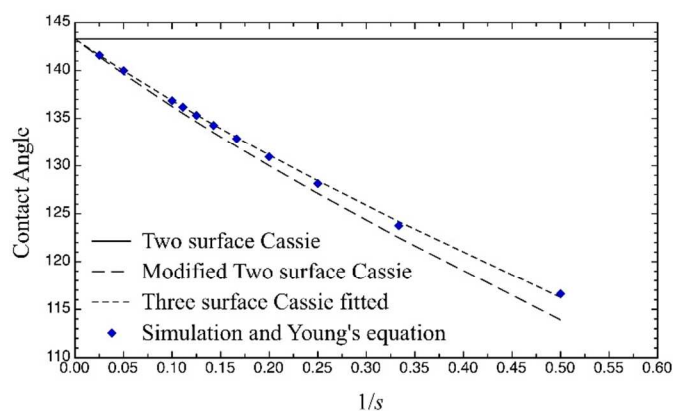


Figure 7. Contact angles (diamonds) from simulation free energies with Young's equation using the SW potential for tall pillar height limits are plotted versus $1/s$. The results using the flat surface contact angle and different Cassie model implementations are also shown. The solid line is the standard two surface model using the actual surface fraction of pillar top (0.25) and the remaining fraction air. The large dashed line modifies the calculation by calculating the pillar surface area as 0.25 plus the fraction of area taken up by lattice sites that adjoin the pillar, $1/s$. The short dashed line used three surfaces, 0.25 for the pillar top, a fitted region whose surface is the adjoining lattice sites, and the remainder of the surface as air.

Discrepancies seen in previous studies

Having studied a much larger range of feature sizes under a number of different boundary conditions, the apparent discrepancies between previous studies using off lattice and lattice density functional formalisms¹⁸⁻²¹ can now be explained as being primarily due to the differences in surface feature sizes and dimensionality of the simulations; one utilized pillars while the other used infinite repeating trenches with sizes of 5σ and 2σ , respectively. The differences were not due to the use of a lattice. A major difference noted between the two studies was the value of the observed contact angle compared to macroscopic model predictions. The work presented here demonstrated that this value is dependent on the feature size and contact path line represented in the simulations. The use of a feature size more similar to the off lattice value will account for much of the noted difference. In addition, the method of calculating contact angles can introduce differences in reported values. Producing droplets that approach the macroscopic limit allowed for determination of this contribution so that either the correct large droplet limit would be approached or a correction can be made when comparing values from studies that use different methods to compute the contact angle. The lattice model can reproduce all of the hydrophilic surface wetting behaviours observed in the off lattice method.

Conclusions

This study sought to understand whether lattice DFT methods could be used to provide increased understanding of contributions to noted deviations in contact angle from predictions of traditional models, specifically, as droplet and feature sizes become smaller. Overall, it has been concluded that it is possible to use lattice DFT methods but care must be taken with several aspects of the model used. An important aspect was evaluation of the various methods utilized for calculation of contact angles from DFT solutions. For

different methods, 3D and p2D flat surface DFT solutions gave results that were consistent but not identical with one another. Directly comparing 3D to p2D to true 2D rough surfaces is not possible because different contact path lines are represented in each case. It is possible to establish bounds for 3D from p2D cases by considering configurations that represent the shortest and longest contact path lines. It was found that the method utilized for contact angle calculation from droplets was important. The correct method provides a limiting contact angle for 3D and p2D DFT solutions as droplet size increases that approaches the value obtained from DFT free energies with Young's equation.

Line tension contributions and ratios of surface feature to droplet size were expected to cause deviations from macroscopic model predictions; this was confirmed by the study presented here. For a flat surface, the DFT solutions depended on droplet size as predicted by other theories. Contact line tension was found to be important only for the smallest of nanodrops, has the predicted dependence on radius, and depends on the droplet shape and interaction potential. The other important aspect, which is the type of surface potential, had no effect for flat surfaces and only became important when surface roughness was introduced. It was clearly demonstrated in these cases that the type of surface potential used influenced the observed behaviours. Small droplets subjected to the SW potential qualitatively followed the behaviour predicted by Wenzel and Cassie-Baxter models based on the flat surface interaction while those subjected to the LJ potential did not; line tension and ratios of feature to droplet size are responsible for a portion of the deviation. The simple SW potential has a very small transition region, and the interaction strength of the pillars does not depend on their size. The LJ potential (and for that matter any real potential) contributes to interactions at much greater distances. The surface interaction of very small pillars will be weaker than the interaction strength of a flat surface.

The behaviour of the LJ potential highlights the contributions of another factor (besides line tension and the ratio of surface feature to droplet size) leading to deviations from macroscopic model predictions. These behaviours were observed in previous studies but the complete implications were not demonstrated by the limited conditions studied.^{18, 19} In fact, these effects arise even when Young's equation is utilized with DFT free energies in calculation of contact angles, meaning even macroscopic droplets would experience the effect. The cases modelled found that the contact angle will be dependent on feature size with the effect becoming noticeable at very small feature sizes. For the SW potential, a simple approximation using a three surface Cassie-Baxter model accounted for the majority of the dependence of contact angle on feature size. This approach identified an increasing percentage of interactions accounted for by the transition region as feature sizes were decreased resulting in larger deviations in the contact angle. This transition-type interaction should also play a role for surfaces interacting with more realistic potentials such as the LJ potential. Only the smallest features exhibited this effect, paralleling the effect of line tension which is only a significant contribution for very small drops. In contrast to line tension effects, the behaviour does not depend on the size of the droplet but rather the fraction of the surface that is transition region so this effect will also be seen for macro-scale droplets.

The influence of small feature size leads to an interesting phenomenon in which it is possible for a nano rough surface to be non-wetting ($>90^\circ$) while the wall-fluid interaction is otherwise wetting on a flat surface ($<90^\circ$). As the surface feature size increases and the pillar surface potential becomes closer to that of the flat surface, the behaviour transitions to that predicted by the macroscopic model. Also, as the wall potential becomes more

strongly wetting, a transition to predicted macroscopic model behaviour occurs for even the smallest surface features. The LJ potential (and other more realistic potentials) fails to uphold basic assumptions inherent to the macroscopic models for a much larger range of features. The transition from wall interaction to fluid filled region under these potentials has a characteristic length, and the interaction at a surface location (depends on the size and location of features) is very different from the flat surface interaction when features become small. Considering these observations together it can be concluded that the observed deviations from macroscopic models for nanodroplets on nano rough surfaces are the result of three contributing factors: line tension contributions, the ratio of droplet size to surface feature size, and variation in surface potential from the flat surface values due to the small feature size. This is an important consideration for devices made with very small feature sizes as models for behaviour built on the macroscopic models will fail even for large droplets.

Because there are several causes for deviations from macroscopic behaviour for drops on nano rough surfaces, care must be taken in drawing conclusions based on the behaviour of models that do not fully explore variations in feature sizes. We have demonstrated that the level of detail in the wall-fluid interaction is a more important consideration than the level of detail in the fluid-fluid interaction. While the fluid comprising the droplets considered for this model does not include hydrogen bonding or electrostatic interactions, the lattice method is capable of producing behaviour that qualitatively matches more realistic fluid potential studies and is an excellent tool to apply to understanding the wetting behaviour for even more complicated surface structures. In a broader context, it is necessary to note the limitations of varying modelling approaches. Lattice models, such as the one applied here, provide qualitative descriptions utilizing a few critical features to maximize the phase space or system size that can be sampled with fixed resources. This provides the opportunity to observe the range of behaviours possible, but does not provide the quantitative or predictive capabilities of some detailed (off-lattice) models. The approach provides a bridge between molecular-scale calculations and macroscopic approaches.

Acknowledgements

Funding for this research was provided by the Office of Naval Research through the US Naval Research Laboratory and by the US Defense Threat Reduction Agency (DTRA), Basic and Supporting Science Directorate (BRCALL07-C-2-0041). The opinions and assertions contained herein are those of the authors and are not to be construed as official or reflecting the views of the US Navy, US Department of Defense, or the US Government.

Notes and references

^a Center for Bio/Molecular Science & Engineering, Code 6900, Naval Research Laboratory, Washington DC 20375, USA.

† Electronic Supplementary Information (ESI) available: results for additional surface and droplet variations; calculated contact angles based on Cassie-Baxter and Wenzel Models as well as the DFT solution free energies; additional isodensity surfaces. See DOI: 10.1039/b000000x/

1. T. Young, *Phil Trans R Soc Lond*, 1805, **95**, 65-87.

2. B. A. Pethica, *Journal of Colloid and Interface Science*, 1977, **62**, 567-569.
3. V. S. Veselovski and V. N. Pertchov, *Zh. Fiz. Khim.*, 1936, **8**, 245-259.
4. A. Marmur, *Journal of Colloid and Interface Science*, 1997, **186**, 462-466.
5. A. Marmur, *Soft Matter*, 2006, **2**, 12-17.
6. A. Marmur and B. Krasovitski, *Langmuir*, 2002, **18**, 8919-8923.
7. A. B. D. Cassie, *T Faraday Soc*, 1948, **44**, 11-16.
8. A. B. D. Cassie and S. Baxter, *T Faraday Soc*, 1944, **40**, 0546-0550.
9. R. N. Wenzel, *Industrial and Engineering Chemistry*, 1936, **28**, 988-994.
10. D. Quere, *Reports on Progress in Physics*, 2005, **68**, 2495-2532.
11. D. Bonn, J. Eggers, J. Indekeu, J. Meunier and E. Rolley, *Reviews of Modern Physics*, 2009, **81**, 739-805.
12. C. Dorrer and J. Ruhe, *Soft Matter*, 2009, **5**, 51-61.
13. P. S. Swain and R. Lipowsky, *Langmuir*, 1998, **14**, 6772-6780.
14. G. Wolansky and A. Marmur, *Langmuir*, 1998, **14**, 5292-5297.
15. C. Dorrer and J. Ruhe, *Langmuir*, 2007, **23**, 3820-3824.
16. L. C. Gao and T. J. McCarthy, *Langmuir*, 2007, **23**, 3762-3765.
17. A. Marmur and E. Bittoun, *Langmuir*, 2009, **25**, 1277-1281.
18. G. O. Berim and E. Ruckenstein, *Journal of Chemical Physics*, 2008, **129**, 014708.
19. G. O. Berim and E. Ruckenstein, *Langmuir*, 2009, **25**, 9285-9289.
20. L. Joly and T. Biben, *Soft Matter*, 2009, **5**, 2549-2557.
21. F. Porcheron and P. A. Monson, *Langmuir*, 2006, **22**, 1595-1601.
22. A. P. Malanoski and F. van Swol, *Physical Review E*, 2002, **66**, 041603.

Author Biographies



Dr. Anthony P. Malanoski received his PhD degree (1999) in Chemical Engineering at the University of Massachusetts Amherst, MA in the research group of Peter Monson. After postdoctoral work at the University of New Mexico and Sandia National Labs in New Mexico with Frank van Swol, he began in 2003 to work at the Naval Research Laboratory first as a National Research Council (NRC) research associate and then in 2005 as a full time employee. His current research interests include thermodynamic and kinetic reaction modelling of nano-scale systems and metagenomic bioinformatics.



Dr. Brandy J. Johnson received a Doctoral degree in Photonics (2004) from Oklahoma State University based on research directed at the application of porphyrins and enzymes in chemical detection under the supervision of H. James Harmon. Since joining the Naval Research Laboratory's Center for Bio/Molecular Science and Engineering in 2004, she has pursued research focused on development of materials incorporating indicators and catalysts within nanoporous frameworks for application to environmental monitoring and self-decontaminating materials. She holds two patents in this area and has numerous publications on the topic.



Dr. Jeffrey S. Erickson received Masters and Doctoral degrees in Chemical Engineering from Johns Hopkins University. Since joining NRL in 2004, his efforts have focused on maturing bench-scale research developments into portable devices and bringing them from laboratory to field incorporating both traditional and monolithic "lab-on-a-chip" style technologies. Dr. Erickson has experience in microfabrication, off-breadboard optical design, microfluidics, electronics, firmware design, and software. In addition, he has written simple GUIs and has packaged instruments into custom housings. He has more than 24 peer-reviewed publications (>529 citations).

This study examines lattice density functional theory as applied to a pillared surface for evaluation of wetting behaviours.

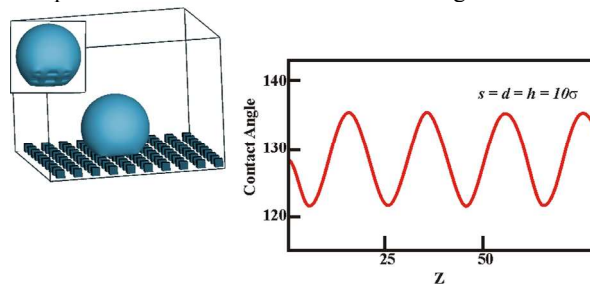


Table of Contents Entry